Next Materials 9 (2025) 101173

Contents lists available at ScienceDirect

Next Materials

journal homepage: www.sciencedirect.com/journal/next-materials

Research article

Comparative analysis of sustainable nanocomposite cellulose nanofiber membranes with polycaprolactone, and polylactic acid

Vishnu Sam [a], Mustehsan Beg [a,*], Keith M. Alcock [a,b]

[a] School of Computing, Engineering & the Built Environment, Edinburgh Napier University, Merchiston Campus, Edinburgh EH10 5DT, UK
[b] Science, Engineering & Aviation, University of Highlands and Islands, UHI Perth, Perth PH1 2XN, UK

ARTICLE INFO

Keywords:
Cellulose nanofiber
Polycaprolactone
Polylactic acid
Membrane
Eco-friendly
Sustainable

ABSTRACT

This study presents sustainable membranes prepared from cellulose nanofibers (CNF) using a simple solution-casting method, focusing on the incorporation of low weight percentages (1 %, 2 %, and 4 %) of polycaprolactone (PCL) and polylactic acid (PLA) to compare membrane performance. The nanocomposite membranes were evaluated based on thickness, wettability, electrolyte uptake, porosity, thermal behaviour, and mechanical properties. The results indicate that CNF-PCL membranes exhibit superior mechanical flexibility and stress tolerance but lower thermal stability, with a glass transition temperature (T_g) of 34.39 °C at 1 wt%, compared to CNF-PLA's T_g of 144.15 °C at the same concentration. The higher crystallinity and greater hydrophilicity of PLA enhance its stability. Additionally, CNF-PLA membranes demonstrate better interfacial compatibility due to hydrogen bonding between PLA's ester linkages and cellulose's hydroxyl groups, improving dispersion, liquid uptake, and overall hydrophilicity (34.66° for CNF-PLA vs. 72.64° for CNF-PCL at 1 wt% loading). These properties make CNF-PLA membranes more resistant to plasticisation and better suited for high-temperature applications. These findings highlight the crucial role of polymer selection and concentration in optimising CNF-based membranes for specific applications.

1. Introduction

Over the past two decades, global energy consumption has increased significantly, driven by rapid technological advancements and economic growth. As a result, the demand for efficient energy production and storage systems has reached unprecedented levels. Currently, energy production primarily relies on fossil fuels, nuclear power, and renewable energy sources. However, the expansion of energy production and storage technologies has led to considerable environmental challenges, including greenhouse gas emissions and ecological degradation. To mitigate these adverse effects, there is a growing global commitment to adopting renewable energy sources and developing biodegradable, eco-friendly materials for sustainable applications across various industries. Consequently, scientists and researchers are prioritising sustainable production methods, the use of environmentally friendly materials, and the reduction of greenhouse gas emissions. Biomass and cellulose-derived resources are gaining significant attention as essential components in a wide range of applications, as well as in the development of various sustainable materials. As the most abundant natural polymer on the planet, cellulose offers a renewable, biocompatible, and cost-effective green resource. Its unique properties, including high mechanical strength, biodegradability, and versatility, make it an ideal candidate for applications in energy storage, sensing devices, and sustainable material development. The increasing demand for eco-friendly alternatives to synthetic materials has further accelerated research into cellulose-based technologies, paving the way for innovative and environmentally responsible solutions in the energy sector [1]. Cellulose nanofibers (CNFs) are ultra-fine fibres derived from cellulose, the primary structural component of plant cell walls, with diameters typically ranging from 5 to 20 nanometres and lengths extending to several micrometres [2]. Due to their high surface area, mechanical strength, and biodegradability, CNFs have gained significant attention in various applications, including energy storage, biomedical engineering, water purification, and sustainable packaging, among others [3]. polycaprolactone (PCL) is a synthetic, biodegradable polyester known for its flexibility, biocompatibility, and ease of processing. It undergoes hydrolytic degradation, which is further accelerated by microbial enzymes, making it suitable for environmentally friendly applications. Notably, PCL's film-forming properties and biodegradability make it a promising candidate for use in membranes for energy storage, providing a

* Corresponding author.
E-mail address: mustehsan.beg@napier.ac.uk (M. Beg).

https://doi.org/10.1016/j.nxmate.2025.101173
Received 28 May 2025; Received in revised form 15 August 2025; Accepted 3 September 2025
Available online 9 September 2025

sustainable alternative for eco-friendly energy devices [4]. Similarly, Polylactic acid (PLA), a biodegradable thermoplastic polymer derived from renewable sources such as corn starch and sugarcane, is widely used in packaging, agriculture, and biomedical applications due to its excellent mechanical properties and environmental sustainability [5].

In addition to their environmental benefits, CNFs demonstrate exceptional mechanical strength, with tensile strengths reaching up to 1.57 GPa and elastic moduli in the range of 140–220 GPa. This unique combination of strength and biodegradability enables the development of durable yet environmentally friendly material [6]. The abundant hydroxyl groups on CNF surfaces enhance hydrophilicity, promoting water absorption and microbial activity, which further contributes to degradation. Studies have shown that CNF-based coatings can degrade by up to 97 % within seven days under composting conditions, highlighting their potential for sustainable applications [6]. Furthermore, CNFs can be readily modified or blended with other biodegradable polymers to create composite materials with tailored properties, such as improved barrier performance and controlled degradation rates. These attributes make CNFs highly suitable for biodegradable packaging and other eco-friendly products, supporting the transition towards a more sustainable materials economy [7]. PLA, another biodegradable polymer, offers a promising alternative to conventional plastics. Its chemical structure, composed of ester bonds, facilitates hydrolysis, the initial step in its biodegradation process [8]. PLA's degradation rate is influenced by its structural characteristics, with amorphous regions degrading more rapidly than crystalline ones. Studies have shown that amorphous PLA degrades by 14 % within four months, while crystalline PLA takes about 20 months to reach a similar degradation level [9]. PLA's biodegradation is also temperature-dependent, occurring most efficiently at temperatures above 58°C and relative humidity levels exceeding 70 %. Under these optimal conditions, PLA can biodegrade significantly within 30–60 days. Additionally, PLA's molecular weight plays a crucial role, with lower molecular weight PLA degrading at a faster rate. The polymer's hydrophilicity promotes water absorption, accelerating hydrolysis and enhancing degradation [10]. Beyond hydrolytic degradation, PLA is also susceptible to enzymatic attack by microorganisms, which further break it down into non-toxic by-products such as lactic acid, carbon dioxide, and water [11]. These characteristics underscore PLA's potential in the development of sustainable and biodegradable materials. Similarly, PCL possesses several attributes that support its biodegradability, making it a versatile material for various applications. PCL is a semi-crystalline, aliphatic polyester with a low melting point (60°C), which facilitates its easy processing [12]. Its biodegradation follows a two-phase process: first, molecular weight loss due to chain scission occurs without significant weight loss, followed by a slower chain scission rate and noticeable weight loss [12,13]. This biodegradation is primarily driven by hydrolytic cleavage of ester bonds and enzymatic attack by microorganisms [14]. The semi-crystalline structure of PCL, with amorphous regions degrading faster than crystalline regions, allows for a controlled biodegradation rate. PCL is capable of biodegrading in various environments such as soil, water, and compost, with degradation rates influenced by factors like temperature, pH, and microbial activity [15]. Under optimal conditions, PCL can degrade significantly within months, though in natural environments, the process may span several years. These properties make PCL suitable for applications in medical implants, drug delivery systems, and environmentally friendly packaging materials [14].

Global plastic production has quadrupled with the growing reliance on polymers, driving a sharp rise in greenhouse gas emissions, measured in carbon dioxide equivalents (CO_2e), across their entire lifecycle. By 2050, these emissions are expected to contribute up to 15 % of the world's total carbon budget [16]. The carbon footprint (CF) of cellulose is influenced by its origin, whether sourced from wood or agricultural residues and the processing techniques employed. While natural cellulose polymers generally have a far smaller carbon footprint than synthetic counterparts, both mechanical and chemical pulping are energy-demanding, and the production of nanocellulose requires even greater energy inputs. Reported global warming potential (GWP) values for nanocellulose range from 18.6 to 1160 kg CO_2e/kg at the laboratory scale, compared to 5.6–16.8 kg CO_2e/kg at the industrial scale, highlighting the considerable gap in energy use and efficiency between small-scale research and large-scale manufacturing [17]. One study estimated the carbon footprint for producing chitosan–CNF composite films at about 3.91 kg CO_2e per kilogram of film, a value slightly below that of both fossil-derived low-density polyethylene (LDPE) and bio-based poly(lactic acid) (PLA) films[18].

Although PLA is regarded as a more sustainable option compared to petroleum-derived plastics, its production still carries a moderate carbon footprint because fermentation and polymerization are energy-demanding processes. Furthermore, growing feedstocks like corn or sugarcane involves fertilizer use, irrigation, and potential land-use changes, all of which add to its overall environmental impact. The carbon footprint and 100-year Global Warming Potential (GWP100) associated with the life cycle of polylactic acid (PLA) trays for fresh food packaging have been assessed, with comparisons made to polystyrene (PS)-based trays. Two transportation scenarios were considered for the supply of PLA granules to the tray production facility: transoceanic freight vessel and intercontinental freight aircraft. The study revealed that the GWP100 is mainly driven by the production of PLA granulate and its transportation to the manufacturing site. Depending on the transportation method, the carbon footprint associated with PLA trays can increase to the point where they are no longer more greenhouse gas emission-efficient compared to PS trays. The GWP100 for the system analysed was 4.826 kg CO_2e/kg of packed trays, with the production of PLA granulate accounting for 61.26 % of the impact. The study showed that the GWP100 of PLA trays (4.826 kg CO_2e) is only slightly lower than that of EPS trays (5.11 kg CO_2e), indicating a small difference of 5.5 % between the two types of trays [19]. There is limited information available on the GWP of PCL, which could make it an interesting area for future research.

Recent advancements in nanocellulose-based aerogels have propelled the development of eco-friendly and high-performance air filtration materials, addressing global concerns over pollution and sustainability. Sepahvand et al. evaluated the fabrication process, modification techniques, and processing of cellulose nanofiber (CNF)-based aerogels and their potential applicability in particulate matter (PM) or CO_2 catchment as they present large specific surface areas, pore structure, and enhanced mechanical properties [20]. In complementary studies, bacterial cellulose aerogels immobilized with reactive silane compounds have been shown to improve their PM removal rate more than 95 %, with chitosan-integrated aerogels better than 99.5 % filtration efficiency of PM2.5 with enduring stability [21]. Furthermore, the introduction of additional substances, including zeolitic imidazolate frameworks and carbon dots with nanoscale size elements, endows cellulose-based filters with new antibacterial features and multifunctionality, which significantly increases their range of use [22]. Although these results are encouraging, obstacles are still present in the industrialization of such structures based on many-body interactions, achieving mechanical stability, and the trade-off between porosity and filtration performance in practice. Recent developments in hybrid material construction, green manufacturing technology, and life cycle analyses suggest that a sustainable, biodegradable, multifunctional aerogel filter with strict environmental and functionality standards will evolve in the future [23].

Biodegradable nanofiber filters were developed using surface-modified CNFs substituted with graphene oxide (GO) in a promising pathway to removing particulate matter (PM) in the air effectively and sustainably. Ashori et al. (2024) recently described the manufacture of CNF-GO nanocomposites through the ultrasonic substitution of CNFs with 0.5–1.5 wt% GO and freeze-drying to obtain light weighted, porous aerogels. Such CNF-GO filters showed excellent PM capture efficiencies that ranged between 86.37 and 99.98 (w/w) with increasing GO loading

up to 1.5 wt./wt., which has been attributed to the large specific surface area, large amount of oxygen-containing functional groups on GO and its entrapment of particles by its nanoplatelet morphology. It was observed that GO addition enhanced thermal stability with minor depressions of porosity and surface area attributable to the filling of pores. Although there was partial loss of biodegradability upon addition of GO, the filters did exhibit significant degree of degradation in soil conditions, a factor that portrays their sustainability. The study highlighted the balance between mechanical robustness, filtration efficiency, and biodegradability in designing next-generation green air filters [24]. This aligns with other research demonstrating that GO modification enables uniform and hydrophilic surfaces, which promote efficient and stable PM2.5 adsorption, crucial for airborne pollutant control [25,26]. The increase of hydrophilicity and dipole interactions of particulate aerosols also assist in capturing and retention on the cellulose nanofibers due to the oxygen-containing groups on the surface of GO. Synthetic polymer-based filters are inferior in some respects such as being biodegradable, light weight, tuneable by tailoring the surface chemistry and composition to such nanofiber filters. There are still capabilities needed to scale up production and to optimize pore structure to not compromise porosity or biodegradability, but the combination of CNFs and GO will enable sustainable and high-performance air filtration materials equal to the challenge of pressing environmental and health problems [27].

Fazel et al. offer a sustainable and effective way to achieve the oil - water separation using CNF aerogels by examining the improvement of the oil adsorption capacity with surface hydrophobization of cellulose nanofiber (CNF) aerogels, by hexadecyltrimethoxysilane (HDTMS). Treating CNF aerogels with optimized HDTMS concentrations, especially at an optimal 2 mL loading, allowed the authors to increase dramatically the hydrophobicity of the surface and enhance the pressure resistance of the material without and altering the lightweight nature and oil sorption capacity of the aerogel. Salinization steps also caused significant morphological alterations, including the decrease in the pore size and pore wall thickening, and a more distinct change in the native hydrophilic character of CNFs to a highly hydrophobic character. These constructed morphological and topographical features facilitated selective oil absorption by pushing water away, thus the material would prove very useful in the less favourable oil spill clean-up environments. Moreover, the mechanical stability increased as well, which made it possible to recycle it after a series of adsorption and desorption processes and create long-lasting absorbents [28]. This method is in line with more general trends in the study of nanocellulose aerogels, where chemical surface modification has proved capable of dramatically enhancing oil selectivity and long-term stability, most commonly through alkyl or fluoro-silane treatments. More precisely, modification of HDTMS is also useful as it can attach long chains of hydrophobic molecules to cellulose surfaces thus reducing surface energy and affinity towards nonpolar hydrocarbons. In comparison to unmodified CNF aerogels, the HDTMS modified materials showed improved sorption rates and retention rates upon compression and structural robustness in wet conditions, some of the main drawbacks that otherwise hamper the possible use of bio-based absorbents. The study of Fazel et al. is a step towards the attainment of scalable, cost-effective, and environmentally friendly remediation solutions that can decrease oil contamination in marine and industrial environments by introducing biodegradable substrates into the picture [28].

Titanium dioxide (TiO_2) nanoparticles-modified CNF aerogels have been designed as functional nanofiltration materials capable of removing PM with extraordinary high performances. 1–2.5 wt% of TiO_2 nanoparticles within CNF aerogels using citric acid cross-linking and freeze-drying methods also produced aerogels with better characteristics such as higher density (11.8–19.7 mg/cm 3), elevated specific surface area (287–370 m 2 /g), as well as greater mechanical strength indicated by a larger young modulus (33.5–125.5 kPa). The TiO_2 treatment was also successfully used in decreasing the pore size (20.2 nm to 15.6 nm) and porosity (99.6 percent to 97.7 percent), thus leading to the positive filtration performance. Subsequently, these aerogels removed 100 percent ultrafine particulates whose size fell within 0.1–5 m range at 2.5 wt% TiO_2 loading. Notably, even after such improvements, the CNF-TiO_2 aerogels still exhibited their intrinsic biodegradability as more than 70 per cent degraded in the first month of burial in soil thereby indicating its sustainability as a green filtering media. Such a combination of enhanced filtration efficiency and mechanical strength with eco-friendliness makes TiO_2 -functionalized CNF aerogels potential replacements of current synthetic filters in the field of advanced air filtration and nanofiltration [29]. Further studies confirm the results in TiO_2 nanoparticles enhancing both filtration through the reduction of pore size and elevation of adsorption sites and, added, lending the aerogels photocatalytic abilities to degrade pollutants in the presence of light, conceiving potential dual-purpose filters with the ability to degrade pollutants when the filters are exposed to light. The given cross-linked arrangement of CNFs allows excellent dispersion of TiO_2 and maximizes its contact with particulate impurities, an additional factor that increases filtration efficiency. This is because TiO_2 and CNF provide a synergy that makes the filtered lightweight, porous, and mechanically sturdy filters that have the multifunctional capability of air purification [30].

A recent study has pointed at the emerging potential in terms of biocompatible nanofiber composite and skin hydration and cosmetic use. The patents effectively produced electro spun poly (vinyl pyrrolidone) (PVP)/CNF/Aloe vera composites that have remarkable moisture absorption rates, (up to 1829), porosity (ranges between 86 and 93), and fibroblast viability of more than 98 percent, revealing good biocompatibility and capability to hydrate facial masks. The Aloe vera powder also enhanced homogeneity and flexibility of fibres without detrimental effect on mechanical properties, and these composites allow contacts with skin. In parallel with this research, another research study by Wang et al. synthesized poly (vinyl alcohol) (PVA)-based facemask nanofibers with natural and bioactive items, including honey and eggshell membrane using environmentally friendly electrospinning applications. These masks showed over 400 percent water absorption, enriched antioxidant potential, and antibacterial action in favouring skin hydration, protection, and preservation with no synthetic preservatives being used [31]. On the same note, Liu et al. reported on CS/PVP nanofiber membranes having chlorogenic acid, which exhibited increased hydrophilicity, faster wound healing, and antimicrobial properties to establish the legitimacy of biopolymer mixtures and plant extracts in modern skin care fabrics [32]. These studies collectively highlight on the increased adoption of the use of cellulose nanofibers and natural bioactive compounds like Aloe vera in polymer nanofibers through electrospinning resulting in composites with multiple features, extreme porosity, and biocompatibility, and are most applicable as a moisturizing and protective facial mask.

Surface modification of CNF aerogels has proven to be an effective strategy for tuning their structural, mechanical, and functional properties for targeted applications. Sepahvand et al. (2020) demonstrated that phthalimide functionalization of CNF aerogels increased surface area and modulus while reducing pore size and thermal stability due to hydrogen bond disruption, thereby altering the aerogel's microstructure and performance characteristics [33]. Similar modification approaches have been reported using silane-based treatments. For example, trimethylsilylation of bacterial cellulose aerogels with trimethylchlorosilane produced highly hydrophobic, oleophilic fibres while maintaining high surface area (~169 m^2 g^{-1}) and porosity (~99.6 %), enabling selective oil adsorption without compromising mechanical integrity [34]. Likewise, methyltrimethoxysilane (MTMS) modification of CNF aerogels has been shown to impart strong water repellences while preserving the three-dimensional nanofiber network, thereby maintaining high surface area and porosity for efficient oil–water separation (Wu et al., 2025). Collectively, these studies highlight that targeted chemical modifications—whether via phthalimide incorporation or silane

functionalization—can significantly influence CNF aerogel properties, enabling customized performance for applications such as oil adsorption, hydrophobic coating, and environmental remediation [35].

Hydrogels based on CNF are already actively developed to treat the burn and they possess high values of biocompatibility, structural stability, and wound-healing efficiency. Basti et al. (2022) prepared hydrogel film made of CNF, hydroxyethyl cellulose (HEC), and citric acid, as a cross-linker that would bring about pain relief, in addition to promoting wound healing after burn injuries. They determined that the CNF structure remained intact after fabrication, and cationization of CNFs was verified through FTIR spectroscopy, which helped in the drug absorption and controlled release attributes [36]. The hydrogels tested with the cell viability (MTT test) showed strong biocompatibility and non-toxicity, and, therefore, may be considered as a great alternative to hydrogel burn dressing. Besides, these hydrogels integrated moisture and mechanical resilience, which is essential to ensuring an optimal wound environment favourable to wound healing (Basti et al., 2022) [36]. The potential of CNF hydrogels in wound and burn management is also supported by research. As an example, Baş et al. (2023) described transparent hydrogels prepared with TEMPO-oxidized CNFs of softwoods, which demonstrated robust mechanical behaviour and great fibroblast and keratinocyte biocompatibility levels, required for wound dressing products [37]. These nanofibril hydrogels can support a stable 3D network, in addition to having moisture retention and non-toxicity, which can induce wound healing and tissue regeneration. Furthermore, robust mechanical strengths and broader antibacterial and self-healing properties of the pH-responsive cellulose nanofibril/poly (vinyl alcohol)-based hydrogels described by Yang et al. (2022) promoted faster wound closure and the prevention of bacterial infection. These multifunctional hydrogels prove how the use of bioactive functionalities in CNF-based materials can enhance the therapy of burn wounds and infected skin lesions tremendously [37,38].

In this study, eco-friendly CNF nanocomposite membranes were fabricated using a simple solution-casting method and systematically evaluated for their thickness, wettability, electrolyte uptake, porosity, thermal behaviour, and mechanical properties. Alongside CNF, weight percentages (1 %, 2 %, and 4 %) of PCL and PLA were incorporated to assess their impact on the overall performance of the nanocomposite membranes. This approach provides valuable insights into how polymer composition influences membrane properties, emphasising their potential for various sustainable applications. With the growing focus on biodegradable materials, CNF-based membranes have attracted significant interest due to their sustainability, mechanical robustness, and adaptable surface chemistry, making them promising candidates for next-generation applications. Recent studies have highlighted amorphous CNF-based supercapacitors with enhanced electro adsorption capabilities, making them particularly suitable for compact, portable devices and renewable energy applications [39]. Similarly, PLA and PCL have shown great potential due to their flexibility, biodegradability, and customisable physical properties. Research on PLA/PCL composite membranes, particularly those enhanced with additives like zinc oxide (ZnO) and polyethylene glycol (PEG), has demonstrated improvements in crystallinity, mechanical performance, and thermal behaviour [40]. Advancements in fabrication techniques, such as electrospinning and breath-figure templating, have further facilitated the development of porous membrane structures optimised for energy applications [41]. Review articles on PLA nanocomposites have reinforced their suitability for sustainable energy technologies, while studies optimising the ratio of PCL in PLA/PCL blends have highlighted improvements in electrochemical stability [42]. Collectively, these findings underscore the increasing relevance of CNF, PLA, and PCL-based membranes in the development of biodegradable, high-performance materials for eco-friendly applications [42]. Fig. 1 shows schematic representation of the synthesis process for CNF-PCL/PLA nanocomposite membranes and some of its diverse applications.

2. Methodology

2.1. Materials and fabrication

The materials required for all stages of this project were sourced from Sigma-Aldrich (UK) and Fisher Scientific. Solution casting was chosen as the fabrication method due to its simplicity in producing membranes. Various solvents were tested for their ability to dissolve PLA, including tetrahydrofuran (THF), dimethylformamide (DMF), chloroform, and toluene. However, only DMF was suitable for solvent exchange, making it the preferred choice for preparing PLA nanocomposite membranes. Similarly, PCL was tested with THF, toluene, DMF, and dichloromethane (DCM), with DMF being selected as the optimal solvent for dissolving PCL. Although both polymers were soluble in THF, DMF, and toluene, DMF was ultimately chosen due to its superior compatibility with the solvent exchange process, ensuring uniform dispersion of nanofillers and enhanced film formation.

The method used to prepare the CNF from water hyacinth fiber pulp is developed based on our previous work [43], and is outlined as follows: 60 g of dry water hyacinth powder is soaked in deionized water (DI H_2O) and homogenized for 15 min at 2000 rpm to form a fibre slurry. The DI H_2O is removed by using a 5 μm pore size nylon cloth, and the fibres are soaked in sodium hypochlorite and DI H_2O solution at a 1:3 vol ratio using acetic acid to adjust the pH level to 4. The solution is stirred at

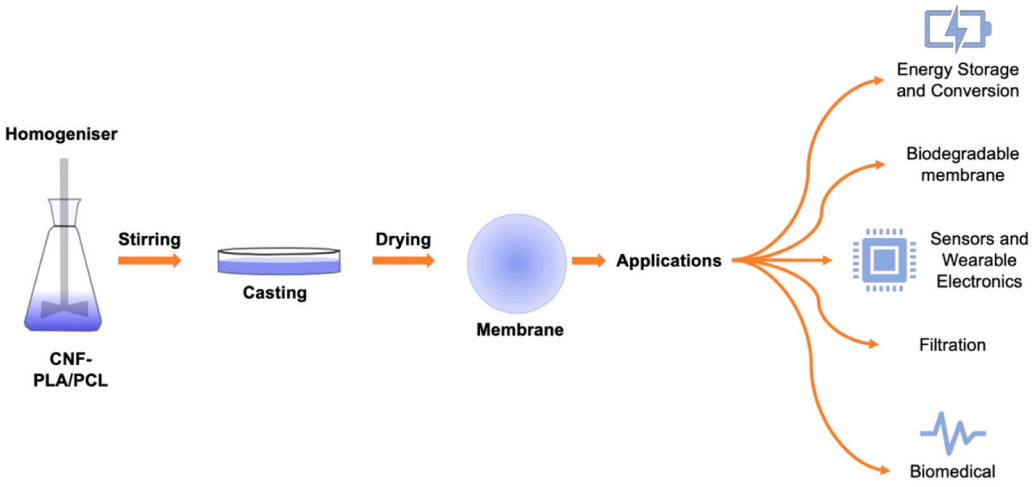

Fig. 1. Schematic illustration of the procedure for CNF-PCL/PLA nanocomposite membranes synthesis and its various applications.

200 rpm and left overnight in a fume hood at 25 °C. The fibres are then washed and filtered using DI H_2O and dried in the fume hood for 2 h, three times. Next, the fibres are soaked in a sodium hydroxide solution for 2 h, washed in DI H_2O, filtered with a nylon cloth, and dried in the fume hood three times. Then, fibres are soaked in sodium hypochlorite and DI H_2O 1:3 vol ratio (acetic acid for adjusting the pH to 4) for 2 h. After washing, filtering using the nylon cloth, and drying the fibres in the fume hood, three more times, the final step is to soak the fibres in DI H_2O and through a microfluidizer using a 200 µm chamber (10 passes) to make the final CNF suspension.

The CNF suspension was dried in the oven at 35 ℃ for 72 h to get a CNF powder. The polymers and DMF were mixed at a 1:10 polymer-to-solvent ratio, with 10 g of polymer dissolved in 100 g of solvent. The mixture was then placed on a magnetic starrier for 24 h to ensure complete dissolution and achieve a homogeneous solution. Once fully dissolved, the polymer solution was mixed with the correct amount of solvent exchanged-CNF for each membrane and the solution was poured into a glass petri dish. It was left in a controlled environment to facilitate the slow evaporation of the solvent. To ensure the complete removal of residual solvent, the samples were left to dry in a fume hood under ambient conditions for 24 h. This step is critical in preventing solvent retention, which could compromise membrane integrity and mechanical properties. Fig. 2 shows the schematic representation of the fabrication process.

2.2. Characterisation

Membrane thickness was measured using digital callipers. Wettability, a key factor in material interactions, significantly influences absorption and compatibility with liquids. Poor wettability can hinder fluid penetration and distribution, potentially affecting overall performance in various applications. Liquid uptake (LU) is directly related to porosity, as a higher pore density improves water absorption, ultimately influencing performance, lifespan, and safety. LU was calculated using Eq. 1 after soaking the membrane in deionised water for four hours at room temperature.

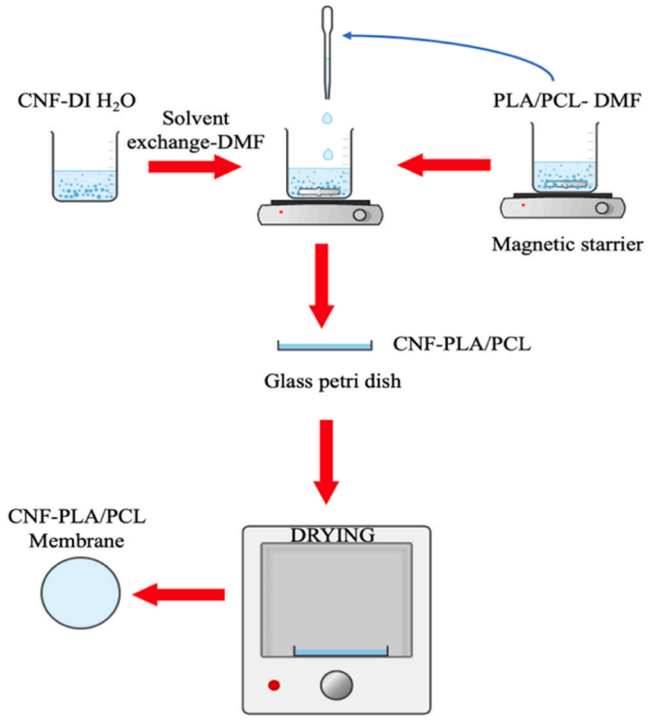

Fig. 2. Schematic diagram illustrating the membrane fabrication process.

$$LU(\%) = \frac{w1 - w0}{w0} \; x \; 100 \quad (1)$$

where w_0 is the dry membrane mass, while w_1 denotes the mass after water absorption. Wettability is influenced by the material's hydrophilicity, with hydrophilic membranes exhibiting superior wettability, whereas hydrophobic surfaces repel liquid. Wettability was evaluated at 25 °C by measuring the water contact angle using AutoCAD Inventor. A contact angle greater than 90° indicates hydrophobicity, while a contact angle less than 90° signifies hydrophilicity. To assess wettability, a droplet of deionised water was placed on the membrane surface, and an image was captured for analysis. Membrane porosity, defined as the ratio of void volume to total volume, was determined using mineral oil absorption and calculated using Eq. 2.

$$Porosity(\%) = \frac{Mw - Md}{pb \times V} \; x \; 100 \quad (2)$$

where M_w and M_d are the wet and dry weights, pb is the mineral oil density (0.87 g/cm^3), and V is the membrane volume. Differential scanning calorimetry (DSC) was performed using a TA Q2000 DSC to analyse thermal transitions, including the glass transition temperature (T_g) and melting temperature (T_m). Membrane samples were cut, weighed using a six-point balance, placed in Tzero aluminium pans, sealed with pierced lids, and heated at a rate of 10 °C/min from 0°C to 350°C. Scanning electron microscopy (SEM) was conducted using a Hitachi 4800 SEM to examine membrane surface topography, texture, and porosity. Samples were cut, mounted on SEM stubs with carbon tape, and sputter-coated with platinum for approximately two minutes to minimise charging effects. Imaging was performed at 5 kV for low-magnification and 15 kV for high-magnification surface morphology analysis, with cross-sectional images captured at an accelerating voltage of 1–10 kV. The air permeability tests are carried out using Gurley Densometers Permeability/Porosity 4190 N + 4320 model (Gurley time in seconds 100 cm^{-3}). The Fourier Transform Infrared Spectroscopy (FTIR) of the samples was obtained using a PerkinElmer spectrometer. Thermogravimetric analysis TGA tests were conducted on a TA Instruments TGA550 at 20°C/minute to 500°C. Tensile testing was carried out using a Lloyd LRX Tensile Tester equipped with pneumatic grips, following the "Plastics-Tensile Test-Until Break" protocol. Membrane samples with a gauge length of 25 mm and a width of 10 mm were tested at a strain rate of 10 mm/min to determine ultimate tensile strength (UTS) and percentage strain. The toughness is calculated using Eq. 3:

$$Toughness = \int_0^{\varepsilon f} \sigma d\varepsilon \quad (3)$$

Where, σ represents the stress, ε denotes the strain, and εf refers to the strain at failure.

3. Results

3.1. Morphology

The scanning electron microscopy (SEM) analysis in Fig. 3 reveals the morphological characteristics of CNF composites blended with PCL and PLA at varying concentrations. In the top row Fig. 3(a–c), CNF-PCL composites exhibit distinct structural changes as PCL content increases from 1 % to 4 %. At 99 % CNF and 1 % PCL Fig. 3(a), the microstructure appears homogeneous, with a continuous CNF network and minimal phase separation, suggesting effective dispersion of the low PCL content within the fibrous matrix. However, increasing PCL to 2 % (Fig. 3b) introduces slight discontinuities, likely caused by the localised aggregation of PCL domains, which disrupts the CNF network. At 4 % PCL Fig. 3(c), phase separation becomes pronounced, with PCL forming discrete spherical domains embedded in the CNF matrix, indicative of

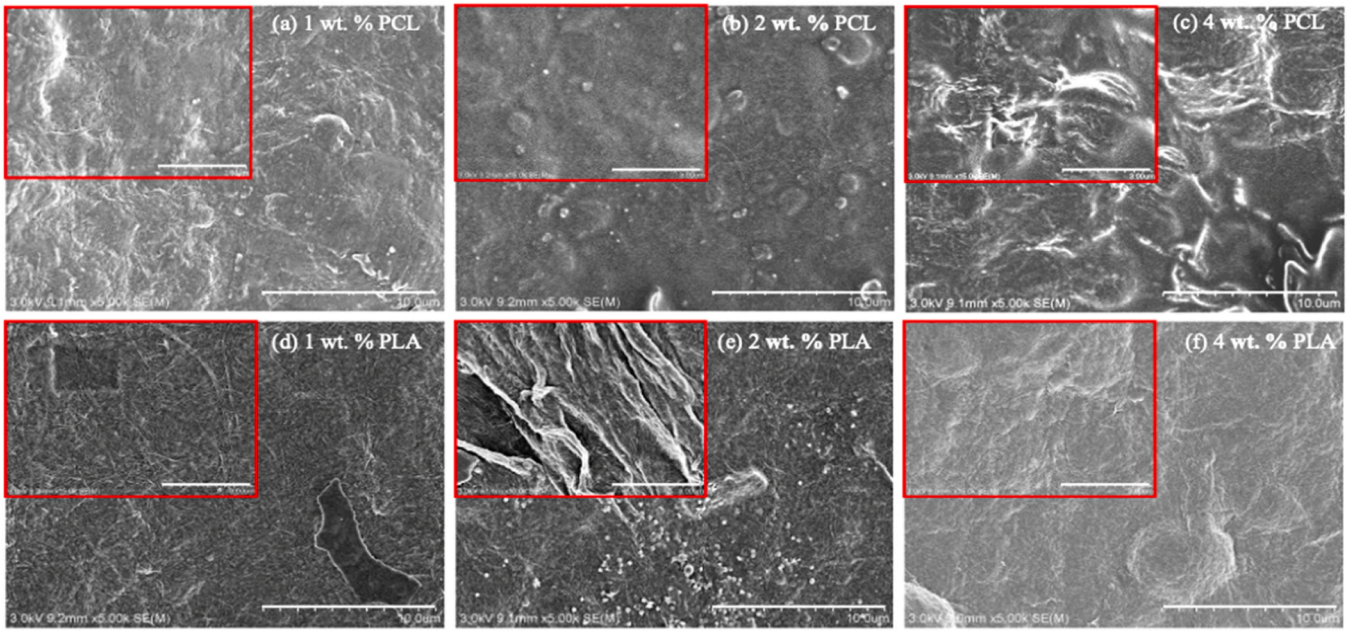

Fig. 3. (a-c) The morphological characteristics of CNF composites blended with PCL and (d-f) the morphological characteristics of CNF composites blended with PLA.

reduced interfacial compatibility at higher polymer concentrations. This inhomogeneity could compromise mechanical integrity, though it may enhance flexibility depending on PCL distribution.

In contrast, the CNF-PLA composites Fig. 3(d–f) display distinct morphological trends. At 1 % PLA Fig. 3(d), the CNF matrix retains its fibrous continuity, with PLA appearing as fine, well-dispersed particles, suggesting favourable interfacial interactions. Increasing PLA to 2 % Fig. 3(e) results in a co-continuous structure, where PLA forms interconnected phases without disrupting the CNF network, which can potentially improve composite toughness. At 4 % PLA Fig. 3(f), however, phase separation emerges, with PLA aggregating into larger clusters, though the overall CNF framework remains more cohesive compared to the PCL counterparts. This implies stronger interfacial adhesion between CNF and PLA, possibly due to polar interactions between CNF's hydroxyl groups (-OH) and PLA's ester linkages (–COO–). The comparative analysis reveals that PLA blends generally demonstrate better compatibility with CNF at higher polymer loadings than PCL. This enhanced compatibility can be attributed to the inherent chemical affinity between cellulose fibres and PLA, as both materials share similar polar characteristics. The hydroxyl groups in cellulose interact more effectively with the ester linkages of PLA, leading to a stronger interfacial interaction and more uniform dispersion of CNFs within the PLA matrix. In contrast, PCL, with its more hydrophobic nature, tends to exhibit weaker interactions with CNFs, especially at higher concentrations. The lack of strong intermolecular forces between PCL and cellulose limits the formation of a stable composite structure, often resulting in phase separation or poor dispersion of the CNFs. This makes PCL-CNF composites more challenging to optimise at higher loadings, though they may still be suitable for applications where flexibility is the primary requirement. The results underscore the important structural role of CNFs and suggest that improving the fibre–matrix interface could lead to further gains in mechanical performance. Recent studies propose several approaches to achieve this, including surface modifications of the CNFs through chemical grafting or physical treatments to improve compatibility with the hydrophobic PCL matrix. One effective strategy is grafting PCL chains onto the CNFs via ring-opening polymerisation, which enhances dispersion and interfacial bonding, which, in turn, increases the tensile strength and modulus of the composite [44,45]. Compatibilisers like maleic anhydride grafted PCL (PCL-g-MA) also act as molecular bridges to enhance CNF-PCL interaction, improving mechanical properties such as Young's modulus, tensile strength, and elongation [46]. Additional surface treatments, including alkali treatment and acetylation have proven effective in enhancing fibre-matrix bonding and mechanical strength [47]. These approaches collectively strengthen composites by improving dispersion and bonding, addressing the mechanical drawbacks indicated by phase separation in SEM images, and reinforcing the scientific rigor of the material design

Surface roughness analysis, quantified by the standard deviation (SD) of height measurements (Fig. 4), reveals distinct trends based on polymer type and concentration within the CNF films. Films incorporating Polycaprolactone (PCL) exhibited relatively high and inconsistent roughness across concentrations (1 wt%: SD = 32.10; 2 wt%: SD = 28.33; 4 wt%: SD = 32.96), showing no clear concentration-dependent pattern. In contrast, films with Polylactic Acid (PLA) demonstrated a significant and consistent reduction in surface roughness with increasing concentration (1 wt%: SD = 28.26; 2 wt%: SD = 24.55; 4 wt%: SD = 23.44). This progressive smoothing effect suggests PLA interacts more favourably with CNFs or facilitates a more homogeneous film formation at higher loadings. Consequently, the 4 wt% PLA composite achieved the smoothest surface overall (SD = 23.44), indicating its potential superiority for applications requiring minimised surface roughness. Hence, reflecting a relatively uniform and low-variation topography. This minimized surface roughness suggests enhanced material homogeneity, which is advantageous for applications where smooth interfaces are critical, such as barrier coatings, biomedical scaffolds, or membranes requiring reduced friction, improved optical clarity, or uniform coating performance.

3.2. *Characterisation*

CNF-based membranes have gained considerable attention due to their biodegradability, high surface area, and tuneable properties. These characteristics focuses on key parameters such as wettability, thickness, liquid uptake, porosity, and air permeability to assess the suitability of these blends for advanced material applications. Wettability analysis (Fig. 5(a-c)) revealed that PCL incorporation steadily increased hydrophobicity, with mean contact angles rising from 72.64° at 1 % to 82.4° at 4 %. This trend aligns with PCL's inherently hydrophobic nature. PLA blends (Fig. 5(d-f)), however, demonstrated a distinct pattern, with a pronounced peak in hydrophobicity at 2 % PLA (65.7°), likely due to

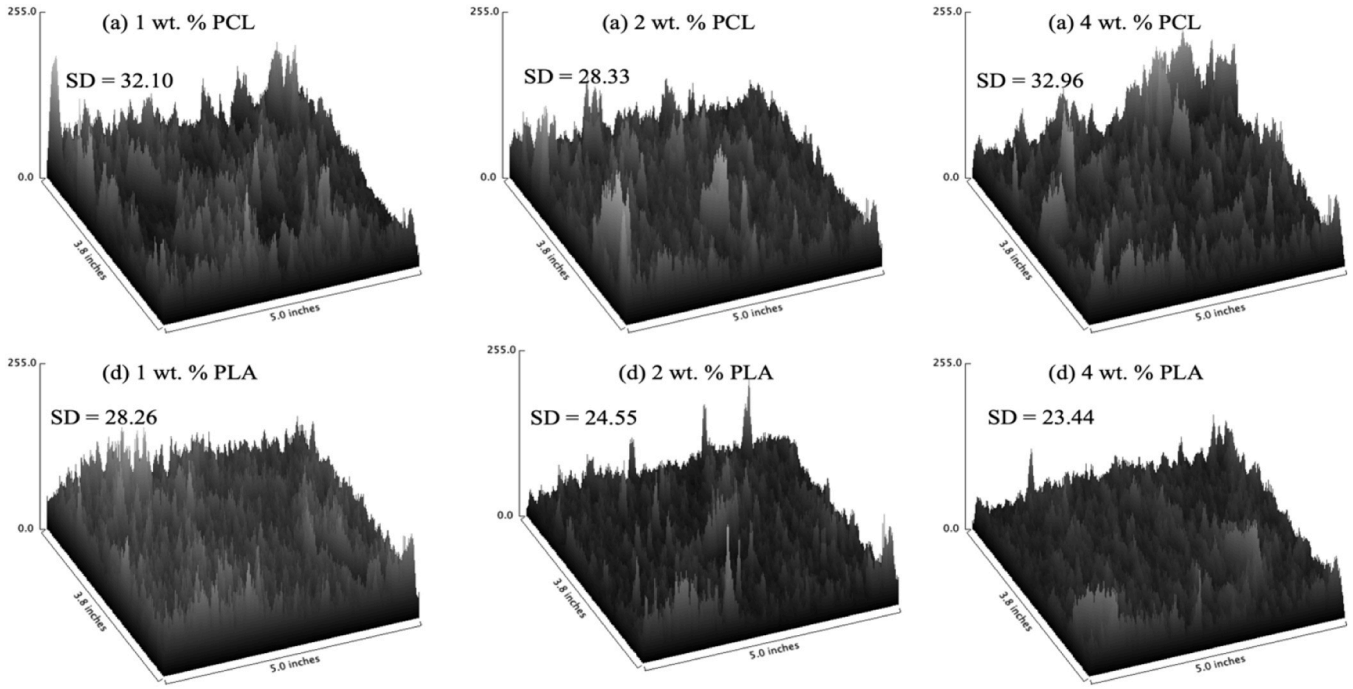

Fig. 4. Surface roughness of the membranes (a-c) for PCL and (d-e) for PLA.

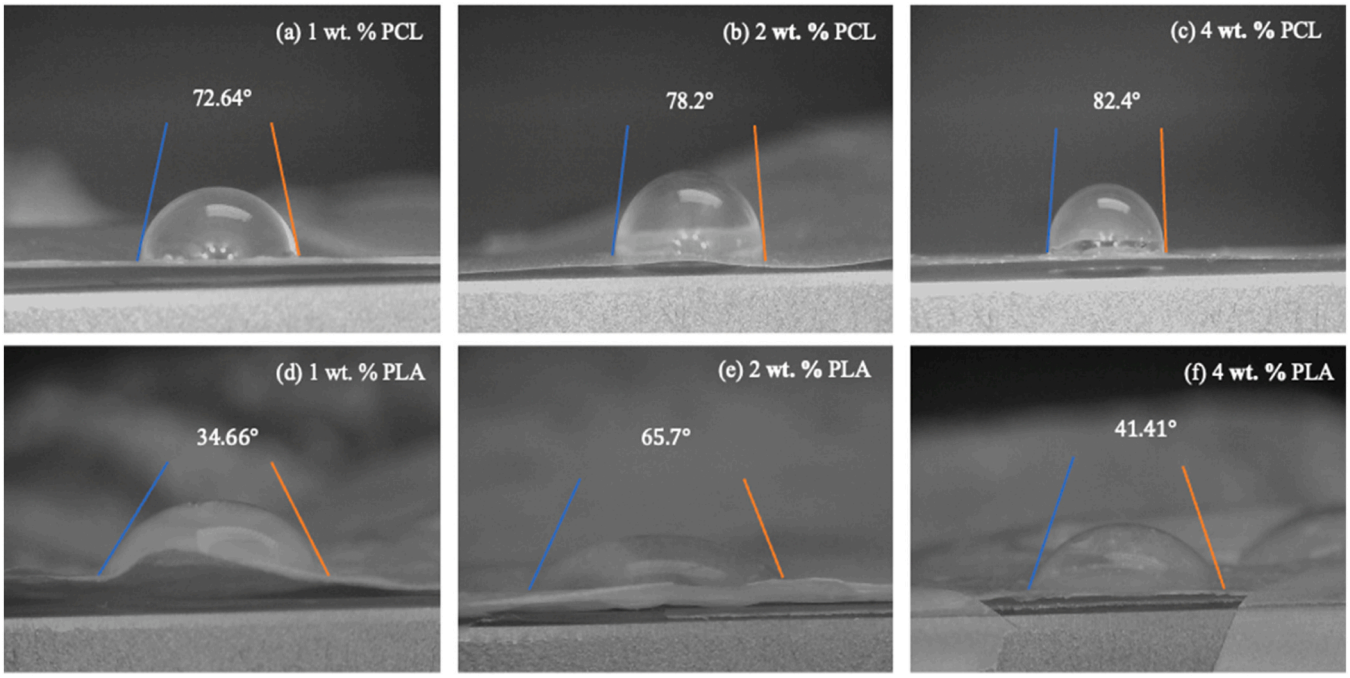

Fig. 5. a-c) Wettability analysis of CNF- PCL membranes and (d-f) wettability of CNF- PLA membranes.

optimal cohesive interactions between PLA and CNF. At 4 % PLA, the contact angle dropped to 41.41°, suggesting phase separation or reduced interfacial compatibility, which may hinder hydrophobic performance. Overall, the CNF-PLA membranes exhibits a more hydrophilic nature compared to the CNF-PCL membranes. This difference in hydrophilicity can be attributed to the inherent chemical characteristics of the two polymers. PLA, with its polar ester linkages and the presence of hydroxyl groups, tends to attract water molecules more readily, enhancing its interaction with moisture. In contrast, PCL has a more hydrophobic backbone due to its non-polar ester groups, which results in lower water affinity.

The thickness (Table 1.) of the membranes varied based on the polymer type and concentration. PCL-blended membranes exhibited a linear reduction in thickness as the PCL content increased, decreasing from 83.3 μm at 1 % to 40 μm at 4 %. This trend suggests that PCL promotes denser packing of CNF, leading to more compact membranes. In contrast, PLA blends showed a non-linear thickness variation, peaking at 40 μm at 1 % PLA, thinning to 30 μm at 2 %, and slightly increasing again to 33.3 μm at 4 %. This irregular pattern indicates potential phase separation at higher PLA concentrations, which may disrupt membrane

Table 1
Membrane characterisation.

Membrane	Thickness (μm)	Wettability (°)	Liquid Uptake (%)	Porosity (%)	Air permeability (Gurley seconds)
PE membrane	20	87.9	111.8	38.77	562.5
1 wt% PCL	83.3	72.6	451.2	33.68	595.5
2 wt% PCL	60.0	78.2	449.4	29.45	629.5
4 wt% PCL	40.0	82.4	173.0	14.68	790.5
1 wt% PLA	40.0	34.6	589.5	41.06	376.3
2 wt% PLA	30.0	65.7	520.4	35.17	533.7
4 wt% PLA	33.3	41.4	485.2	32.70	585.8

uniformity as discussed in Morphology section. Liquid uptake measurements showed (Table 1.) significant differences between the two polymer blends. PCL membranes exhibited high uptake at 1–2 % (approximately 450 %) but experienced a substantial decline at 4 % (173 %), suggesting that higher PCL concentrations led to pore blockage or reduced porosity. In contrast, PLA blends displayed a gradual decrease in liquid uptake, from 589.5 % at 1–485.2 % at 4 %. Despite this reduction, PLA membranes consistently exhibited superior liquid uptake compared to PCL at equivalent concentrations, emphasising better pore retention and overall porosity, as can be seen in (Fig. 6). Porosity and air permeability in Gurley seconds measurements further supported these observations. PCL-blended membranes showed a sharp decline in porosity from 33.68 % at 1–14.68 % at 4 % and increase in air permeability through the membrane from 562.5 to 629.5 Gurley seconds, reinforcing the notion that PCL promotes membrane densification. Conversely, PLA blends started with a higher initial porosity of 41.06 % at 1 %, decreasing moderately to 32.7 % at 4 %. The relatively stable porosity of PLA blends suggests better compatibility with CNF, allowing for the preservation of porous networks even at elevated concentrations. A 1–2 % blend of PLA and PCL revealed that PLA produced thinner, more uniform membranes with superior hydrophilicity at 1–2 %, along with higher porosity and liquid uptake. However, at 4 % concentration, both polymers exhibited reduced performance. Despite this, PLA maintained an advantage in porosity (32.7 % vs. 14.68 %) and liquid uptake (> 485 %). Mechanistic insights suggest that at higher concentrations, PCL forms dense, hydrophobic membranes, which enhances mechanical robustness but compromises porosity and liquid uptake. This makes PCL more suitable for applications requiring structural integrity and moderate hydrophobicity. In contrast, PLA at 1–2 % achieves an optimal balance of hydrophilicity and porosity, making it a promising candidate for wound dressings or controlled-release systems. However, at 4 % concentration, phase separation diminishes PLA's performance, emphasising the need for concentration optimisation. Overall, CNF membranes blended with 1–2 % PLA demonstrate superior hydrophobicity, porosity, and liquid uptake, making them ideal for biomedical and filtration applications. Meanwhile, PCL-blended membranes are better suited for applications prioritising structural compactness, though with trade-offs in permeability. These findings highlight the importance of polymer selection and concentration in tailoring CNF membrane properties.

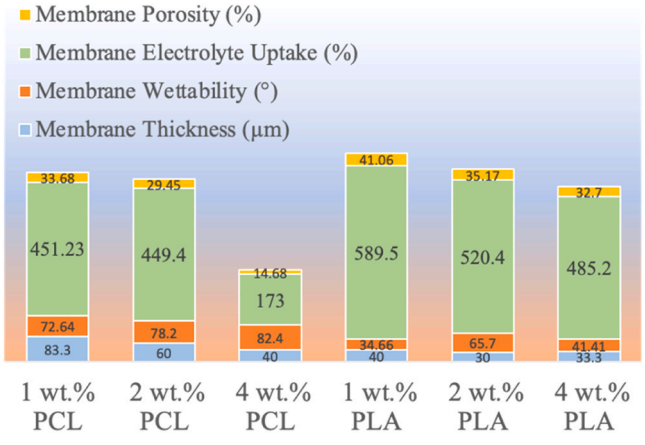

Fig. 6. Graphical representation of Table 1.

3.3. Fourier-transform infrared (FTIR) spectroscopy

Fourier-transform infrared (FTIR) spectroscopy was employed to characterize the chemical structure and interactions within pure CNF, PCL, and PLA membranes as shown in Fig. 7(a), as well as their respective composites. The spectrum of pure CNF exhibits characteristic features: a broad peak cantered at approximately 3300 cm^{-1} attributed to O-H stretching vibrations, C-H stretching bands between 2800 and 3000 cm^{-1} , a peak at ~1640 cm^{-1} indicative of adsorbed water (H-O-H bending), and strong C-O/C-O-C stretching vibrations within the 1000–1100 cm^{-1} region [48]. Pure PCL displays a dominant ester carbonyl (C═O) stretch at ~1720 cm^{-1} , asymmetric and symmetric CH_2 stretches near 2940 cm^{-1} and 2865 cm^{-1} , and key C-O-C stretches at ~1240 cm^{-1} (asymmetric) and ~1165 cm^{-1} (symmetric) [49]. In contrast, pure PLA shows its characteristic ester carbonyl stretch at a slightly higher wavenumber (~1750 cm^{-1}), CH_3 asymmetric stretching near 2995 cm^{-1} , complex deformation bands between 1450 and 1380 cm^{-1} , and prominent C-O stretches around 1180 cm^{-1} and 1085 cm^{-1} [50].

Spectroscopic interrogation of the CNF-based composites revealed successful integration of both PCL and PLA into the CNF matrix. The composite spectra are overwhelmingly dominated by the CNF signature, confirming its role as the continuous phase as shown in Fig. 7(b). Crucially, the emergence and progressive intensification of the characteristic polyester carbonyl peaks – at ~1720 cm^{-1} for PCL composites and ~1750 cm^{-1} for PLA composites – with increasing polymer loading (1 wt% < 2 wt% < 4 wt%) provides definitive evidence for the incorporation of PCL and PLA within the CNF network. Furthermore, alterations in the O-H stretching region (~3300 cm^{-1}) of CNF indicate significant interfacial interactions. A pronounced decrease in intensity and potential broadening of this band is observed in all composites, signifying hydrogen bonding (H-bonding) between the hydroxyl groups of CNF and the carbonyl groups of the polyesters. This interaction is corroborated by subtle alterations and broadening of the polyester carbonyl peaks in the composites compared to their pure states. Notably, the suppression of the CNF O-H band is markedly more significant in PLA composites compared to PCL composites at equivalent weight loadings, strongly suggesting that PLA engages in stronger hydrogen bonding interactions with CNF than PCL does. The absence of new absorption peaks confirms that the composites are physical blends stabilized primarily by hydrogen bonding, rather than new chemical compounds. In conclusion, FTIR analysis confirms the formation of CNF/PCL and CNF/PLA composite membranes and demonstrates that PLA exhibits a stronger hydrogen bonding affinity for CNF than PCL.

3.4. The thermogravimetric analysis (TGA)

The TGA and derivative thermogravimetric analysis (DTG) presented in Fig. 8(a) and (b) respectively, provide important insights into the thermal degradation behaviour of pure CNF membranes, PCL, PLA, and

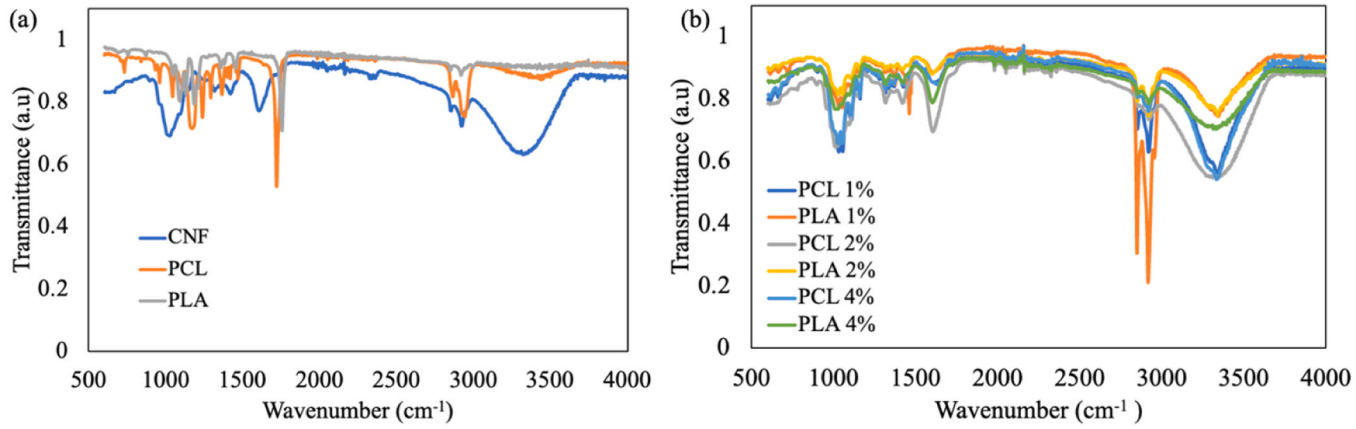

Fig. 7. (a) FTIR analyses on pure CNF, PCL, and PLA and (b) composite CNF membrane.

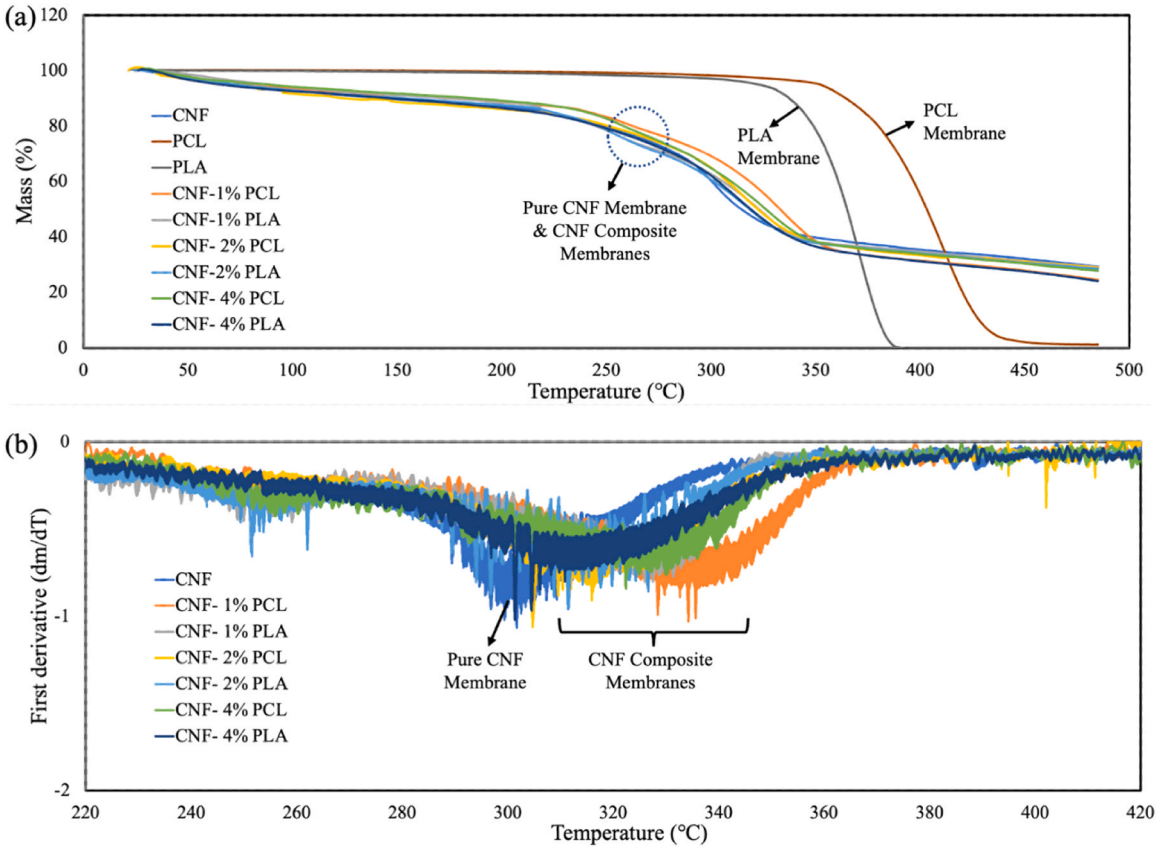

Fig. 8. (a) The TGA analysis of pure CNF, PCL, and PLA membranes and their composites (b) DTG analysis of all the corresponding CNF membranes.

their corresponding CNF/polymer composite membranes. In the TGA curves (Fig. 8(a)), the percentage of mass remaining is plotted against temperature for all samples. Pure CNF membranes and CNF-based composite membranes distinctly exhibit higher thermal stability in comparison to the neat polymer membranes. Up to about 300°C, these CNF-containing samples consistently retain a greater proportion of their original mass, demonstrating the significant thermal resistance imparted by the nanofiber network. In contrast, both PLA and PCL membranes display much sharper mass losses at their characteristic decomposition temperatures with PLA degrading rapidly around 360 °C and PCL at approximately 420 °C. The composites containing increasing concentrations of either PCL or PLA show intermediate stability, confirming that the incorporation of CNF enhances the overall thermal resistance of the blends, likely due to improved interfacial bonding and the reinforcing effect of CNF.

Examining the DTG curves (Fig. 8(b)) further clarifies the degradation events of these materials, highlighting the temperatures at which the most rapid mass loss occurs. Pure CNF membranes display a broad decomposition peak at lower temperatures near 320 °C, illustrating a relatively simple, single-step degradation process. The behaviour of the CNF/polymer composites is distinctly more complex, as evident by multiple overlapping degradation peaks that correspond to the decomposition of both the CNF and the respective polymer phases. The DTG signals of composite membranes are less pronounced and tend to broaden and shift relative to those of the neat polymers, suggesting that the thermal degradation occurs more gradually and over a wider temperature window. This indicates enhanced compatibility between the CNF and the polymer matrices, as well as improved thermal stability

because of the composite architecture.

The results from both TGA and DTG analyses clearly demonstrate that CNF acts as an effective reinforcing and thermally stabilizing phase when combined with either PLA or PCL. The onset of significant thermal degradation is delayed, and the rate and profile of mass loss are modulated in the composites, as opposed to the rapid, singular mass loss of the neat polymers. The introduction of even modest amounts of polymer (1–4 %) into CNF yields a composite with tunable and improved thermal behaviour, underscoring the potential of such materials in applications where controlled degradability and thermal resistance are critical. These findings support the design of advanced, eco-friendly, and high-performance bio composites for applications such as biodegradable packaging, insulation materials, or biomedical devices.

3.5. Tensile strength

The mechanical properties of cellulose nanofibril (CNF)-reinforced membranes blended with PCL and PLA demonstrate significant differences in stress at maximum load (MPa) and strain at maximum load (%), highlighting the impact of polymer selection and additive concentration on overall membrane performance. The virgin PCL and PLA membranes were mechanically fragile and disintegrated before a complete stress–-strain curve could be obtained. For comparison with previous reports, virgin PCL typically exhibits a low tensile strength (~10–15 MPa) but a high elongation at break (>400 %), indicative of its ductile behaviour [51]. In contrast, virgin PLA generally shows a higher tensile strength (~50–70 MPa) but a limited elongation at break (~1–10 %), reflecting its brittle nature [52]. These baseline properties are used to assess the reinforcing effects of CNF in the composite membranes. The result for the pure CNF membrane, as shown in Fig. 9, displays the characteristic response of a stiff and brittle material. The tensile strength data reveal that PCL-based membranes consistently exhibit higher mechanical performance compared to their PLA counterparts as can be seen in Fig. 10 (a) and (b). At 1 wt% concentration, PCL-CNF membranes achieve a stress of 58.34 MPa with a strain of 6.59 %, indicating strong interfacial bonding between CNF and PCL, which promotes both load-bearing capacity and flexibility. However, increasing PCL content leads to a 51.78 % decline in stress (28.12 MPa) and a 30.7 % increase in strain (14.57 %) at 2 wt%, suggesting that excessive PCL dilutes the stress, but strain effect is increased in the membrane. At 4 wt%, stress further drop to 8.9 MPa (51.8 %) and an increase in strain of 7.87 %, respectively. Despite this, PCL membranes consistently outperform PLA-based membranes at all concentrations. In contrast, PLA-CNF membranes exhibit markedly lower mechanical performance due to PLA's inherent brittleness. At 1 wt%, PLA membranes achieve a stress of 26.03 MPa with a strain of 2.65 %, significantly lower than PCL-CNF membranes of the same concentration. At 2 wt%, strain increases to 2.99 %, while stress declines to 21.1 MPa. However, at 4 wt%, stress experiences a sharp

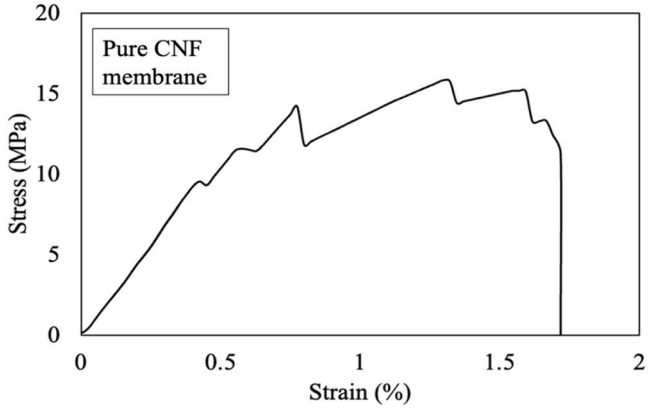

Fig. 9. Stress- strain curve of pure CNF membrane.

8.5 MPa, and strain increases to 3.33 %, indicating severe mechanical degradation likely due to phase separation and weak interfacial bonding.

An analysis of key trends (Fig. 11) reveals that PCL membranes consistently demonstrate superior stress and strain characteristics over PLA membranes compared to PLA, reinforcing its superior mechanical adaptability. PCL's semi-crystalline structure and low glass transition temperature ($T_g \approx -60$ °C) enhance energy absorption, allowing for improved deformation tolerance and flexibility. Furthermore, PCL's elastomeric nature enables stress distribution, reducing the risk of brittle fracture. However, as PCL content increases, stress transfer efficiency diminishes due to its relatively low intrinsic strength compared to CNF. PLA, on the other hand, presents significant limitations. While its higher Tg (~ 60°C) and rigidity may be beneficial for niche applications requiring structural integrity, its poor interfacial adhesion with CNF leads to brittle failure and rapid mechanical degradation. This incompatibility likely stems from hydrophilic-hydrophobic interactions, where CNF's hydroxyl groups struggle to integrate effectively with PLA's hydrophobic polymer chains. Unlike PCL, which exhibits some degree of plastic deformation, PLA membranes fail to distribute stress efficiently, leading to a steep decline in mechanical properties. From a practical standpoint, the results suggest that PCL-CNF membranes are the superior choice for applications requiring strength and flexibility, such as biodegradable packaging and wound dressings. The optimal concentration for PCL is 1–2 wt%, where it maintains a balance between mechanical reinforcement and ductility. In contrast, PLA is best suited for rigid, low-stress applications, such as disposable applications, though even in these scenarios, its performance is inferior to PCL. Higher additive concentrations ($\geq$ 4 wt%) should be avoided for both polymers, as they lead to diminished mechanical properties, with PLA experiencing catastrophic degradation.

Overall, PCL-CNF membranes outperform PLA-CNF composites across all mechanical metrics, particularly at lower additive concentrations. The superior flexibility and stress tolerance of PCL make it a more viable option for most applications, whereas PLA's brittleness and poor interfacial compatibility limit its practical utility.

The toughness of the CNF-based composite membranes, a critical parameter reflecting their resistance to fracture under stress, exhibited a pronounced dependence on both the type and concentration of the incorporated polymer, as detailed in Table 2. Membranes containing polycaprolactone (PCL) demonstrated higher toughness values compared to those with polylactic acid (PLA) at equivalent loadings. Specifically, the toughness of PCL-modified membranes decreased from 5.51 MJ/m^3 at 1 wt% to 4.01 MJ/m^3 at 2 wt%, and further declined to 1.76 MJ/m^3 at 4 wt%. PLA-modified membranes followed a similar inverse relationship between concentration and toughness, but displayed a more significant reduction, falling from 4.99 MJ/m^3 at 1 wt% to 4.71 MJ/m^3 at 2 wt%, and sharply decreasing to only 0.53 MJ/m^3 at 4 wt%. This consistent decline in toughness with increasing polymer concentration for both systems suggests that higher polymer loadings may detrimentally alter the membrane structure or interfacial interactions, leading to increased brittleness. Notably, PCL consistently imparted greater toughness than PLA across all concentrations tested, indicating its potential advantage for applications requiring enhanced mechanical durability.

3.6. Differential scanning calorimetry (DSC)

The thermal behaviour of polymeric membranes, determined by their glass transition temperature (Tg) and melting temperature (Tm), provides crucial insights into molecular mobility, crystallinity, and overall material stability. In this study, membranes composed of PCL or PLA blended with CNFs were analysed to assess how polymer type and concentration influence Tg (amorphous phase mobility) and Tm (crystalline phase stability). The results reveal significant differences between PCL- and PLA-based composites, underscoring their distinct

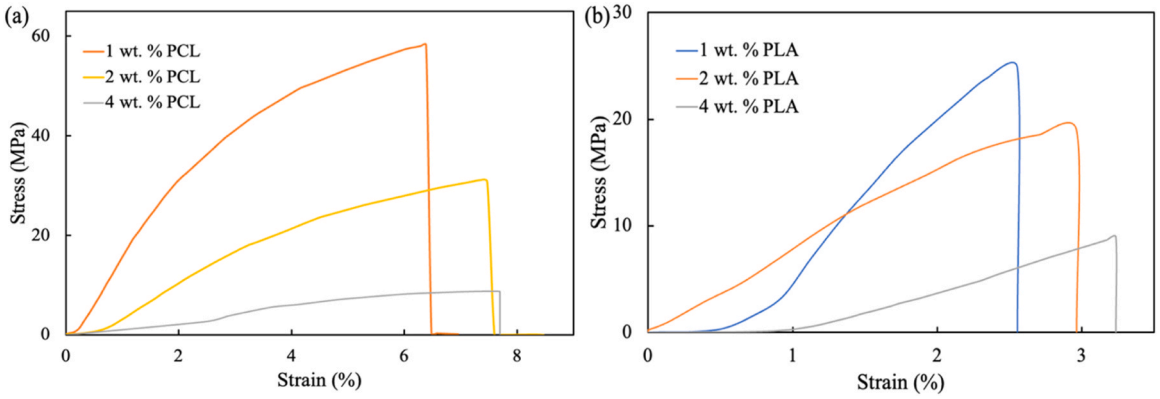

Fig. 10. Stress- strain curves of CNF-based membranes.

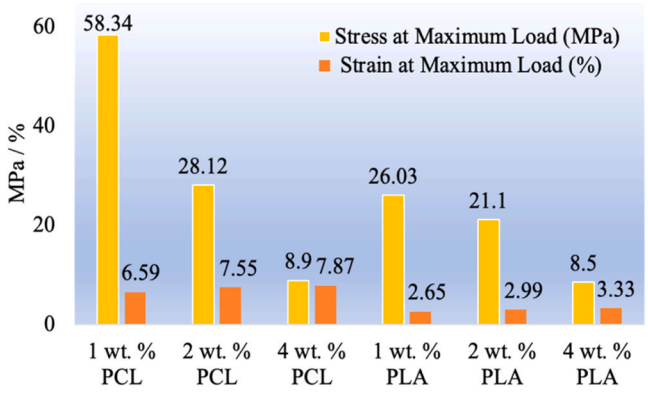

Fig. 11. Graphical representation of the nanocomposite's tensile strength.

Table 2
Toughness results of CNF membrane.

Membranes	Toughness (MJ / m^3)
1 wt% PCL	5.51
2 wt% PCL	4.01
4 wt% PCL	1.76
1 wt% PLA	4.99
2 wt% PLA	4.71
4 wt% PLA	0.53

structure–property relationships (Fig. 12 (a) and (b)).

PLA-based membranes demonstrated pronounced thermal stability, consistent with their semi-crystalline nature. At 1 wt% PLA, Tg and Tm were recorded at 144.15 °C and 145.4 °C, respectively. Increasing PLA content to 4 wt% elevated Tg to 153.5 °C and Tm to 154.22 °C (Fig. 13). The narrow Tg–Tm gap of ~1–2 °C reflects PLAs tightly coupled amorphous and crystalline phases, where structural order extends across both regions. This coupling arises from PLA's flexible aliphatic backbone, which promotes efficient chain packing into crystalline lamellae even at low concentrations. The progressive increase in Tg indicates restricted chain mobility in the amorphous phase due to strong CNF–PLA interfacial interactions, while the concurrent rise in Tm suggests enhanced crystalline phase stability through heterogeneous nucleation at CNF surfaces. At higher loadings (2–4 wt%), the rate of Tg and Tm increase diminished, indicating a crystallisation saturation effect. This plateau likely results from the limited number of nucleation sites at the CNF interface and steric hindrance between tightly packed PLA chains.

PCL-based membranes, in contrast, exhibited much lower transition temperatures, reflecting their predominantly amorphous structure. At 1 wt% PCL, Tg and Tm were measured at 34.39 °C and 77.39 °C, respectively, increasing to 46.47 °C and 93.28 °C at 4 wt%. The large gap between Tg and Tm highlights the dominance of disordered amorphous regions, with crystalline domains forming only at higher temperatures. PCL's relatively rigid backbone and stereochemical irregularities limit chain packing efficiency, resulting in lower crystallinity and broader melting transitions. Its hydrophobic nature may further weaken CNF–PCL interactions, reducing heterogeneous nucleation efficiency. Nevertheless, the linear rise in Tg and Tm with polymer loading suggests gradual improvement in crystalline order as higher PCL content helps overcome kinetic barriers to chain alignment, though this effect remains less pronounced than in PLA.

The contrast in thermal behaviour between PLA and PCL composites is striking. At just 1 wt% loading, PLA reaches a Tg of 144.15 °C—almost 100 °C higher than PCL at 4 wt%—and a Tm of 145.4 °C, exceeding PCL's maximum Tm by over 50 °C. This superior performance stems from PLA's inherently higher crystallinity and greater nucleation efficiency at CNF surfaces, enabling the formation of compact, thermally stable crystalline domains. In comparison, PCL's restricted chain packing and lower interfacial compatibility with CNFs limit crystalline phase development, thereby reducing melting stability. From an application standpoint, CNF–PLA membranes are better suited for high-temperature applications such as filtration and packaging, where stability of crystalline domains is critical. CNF–PCL membranes, while less thermally stable, offer advantages in flexibility and are appropriate for applications such as eco-friendly coatings, where moderate thermal resistance (<100 °C) is sufficient.

The thermal performance gap between PCL and PLA is striking. At 1 wt%, PLA exhibits a T_g of 144.15 °C, nearly 100 °C higher than the 46.47 °C observed for PCL at 4 wt%, while its T_m of 145.4 °C exceeds PCL's highest T_m of 93.28 °C by 52 °C. This disparity arises from the intrinsic properties of the polymers. PLA's high crystallinity, even at minimal loadings, allows for stable crystalline domains that resist thermal disruption, whereas PCL's predominantly amorphous nature limits its thermal resilience. Additionally, PLA's flexible chains facilitate nucleation on CNFs, enhancing crystallisation, whereas PCL's rigid chains hinder efficient packing, further contributing to its lower thermal stability. Also, the variation in Tg observed in the CNF-reinforced membranes can be attributed to the interactions between CNF and the polymer matrix, which restrict polymer chain mobility. Previous studies report a glass transition temperature of approximately ~60 °C for PLA and −60 to – 65 °C for PCL, representing a difference of about ~100 °C, which is consistent with our observations for the CNF–PCL/PLA membrane [53,54]. Hence, CNF-PLA membranes are ideal for high-temperature applications such as filtration and packaging, where thermal stability is crucial. Their ability to achieve a robust T_g and T_m at just 1 wt% minimises material costs while ensuring durability. In contrast, CNF-PCL membranes are better suited for eco-friendly

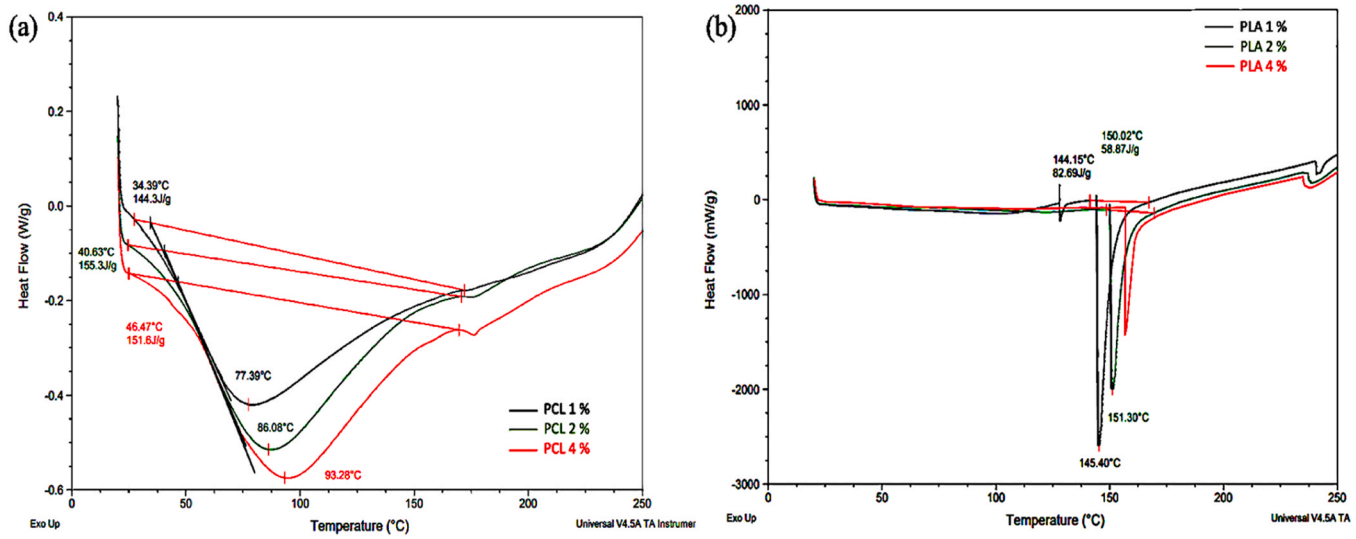

Fig. 12. DSC results of (a) CNF-PCL and (b) CNF-PLA nanocomposite membranes.

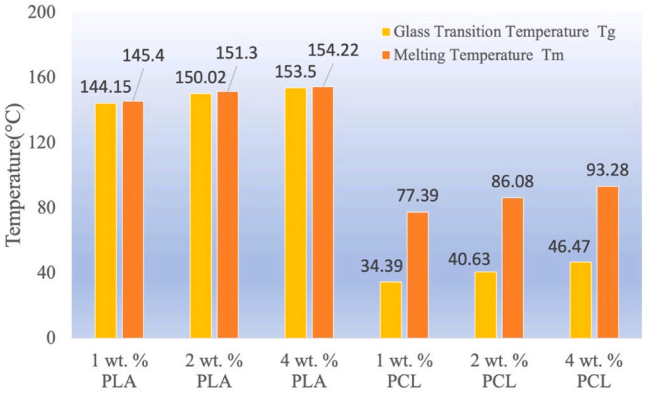

Fig. 13. Graphical representation of the DSC results of the nanocomposite membranes.

coatings, where moderate thermal resistance below 100°C is sufficient.

4. Conclusions

The eco-friendly CNF nanocomposite membranes were prepared a simple solution casting methods and evaluated for thickness, wettability, electrolyte uptake, porosity, thermal behaviour, and mechanical properties. This study highlights the distinct advantages and limitations of CNF-PCL and CNF-PLA membranes, demonstrating how polymer chemistry influences interfacial interactions, mechanical properties, and thermal stability. PLA blends generally demonstrate better compatibility with CNF at higher polymer loadings than PCL. This enhanced compatibility can be attributed to the inherent chemical affinity between cellulose nanofibers and PLA, as both materials share similar polar characteristics. Also, CNF-PLA membranes showed higher hydrophilicity (34.66° for CNF-PLA vs. 72.64° for CNF-PCL at 1 wt% loading) and wettability at all wt% ratios. Despite their weaker compatibility with CNFs, PCL-based membranes can still be optimised for applications where mechanical toughness and compactness are critical. CNF-PCL membranes offer superior mechanical flexibility, at minimal loading concentrations, CNF-PCL membranes outperform CNF-PLA composites across all mechanical metrics, particularly at lower additive concentrations, 1 wt% concentration, CNF-PCL membranes achieve a stress of 58.34 MPa with a strain of 6.59 % compared to CNF-PLA's 26.3 MPa and 2.64 %. The thermal resistance of CNF-PLA T_g of 144.15 °C, nearly 100 °C higher than the 46.47 °C observed for CNF-PCL membrane at 4 wt%. On the other hand, CNF-PLA membranes, with their higher hydrophilicity and better CNF dispersion, are well-suited for applications requiring biodegradability, wettability, and liquid uptake. However, their brittleness limits their performance under extreme conditions.

While the materials and fabrication method appear promising at the laboratory scale, industrial implementation requires consideration of several factors. These include the consistent and cost-effective production of cellulose nanofibers, which can be resource and energy-intensive depending on the extraction method. The incorporation of biopolymers like PLA and PCL must also be evaluated in terms of material availability, processing compatibility, and biodegradability at scale. Furthermore, the solution-casting technique used in the study may not directly translate to high-throughput manufacturing processes such as roll-to-roll coating or extrusion, which are commonly used in membrane or film production. Also, the current study provides comprehensive insights into the properties of CNF-based membranes, challenges remain in balancing mechanical strength, flexibility, and hydrophilicity. Future work could focus on optimising CNF dispersion, exploring hybrid polymer blends, or incorporating plasticisers and crosslinkers to improve toughness without compromising hydrophilicity. Additionally, the high porosity and electrolyte uptake of these membranes suggest potential applications as eco-friendly battery separators in aqueous or non-aqueous electrochemical systems. Further studies are required to evaluate their ionic conductivity, chemical stability, and long-term cycling performance in batteries, as well as scalability for industrial production. Tailoring CNF-polymer interactions and processing methods could enable the development of multifunctional, sustainable membranes for energy storage applications. Overall, these findings underscore the importance of tailoring CNF-polymer interactions to enhance performance in sustainable and functional material applications.

Consent for publication

All authors have given their consent for the publication of this manuscript and its associated materials.

Funding

This research received no specific grant from funding agencies in the public, commercial, or not-for-profit sectors.

Declaration of Competing Interest

The authors declare no competing interests.

References

[1] S. Park, et al., Advances in biomass-derived electrode materials for energy storage and circular carbon economy, Chem. Eng. J. 470 (2023) 144234.
[2] G. Anusiya, R. Jaiganesh, A review on fabrication methods of nanofibers and a special focus on application of cellulose nanofibers, Carbohydr. Polym. Technol. Appl. 4 (2022) 100262.
[3] M. Beg, et al., Paper supercapacitor developed using a manganese dioxide/carbon black composite and a water hyacinth cellulose Nanofiber-Based bilayer separator, ACS Appl. Mater. INTERFACES 15 (44) (2023) 51100–51109.
[4] M. Abedalwafa, et al., Biodegradable poly-epsilon-caprolactone (PCL) for tissue engineering applications: a review, Rev. Adv. Mater. Sci. 34 (2) (2013) 123–140.
[5] N.-A.A.B. Taib, et al., A review on poly lactic acid (PLA) as a biodegradable polymer, Polym. Bull. 80 (2) (2023) 1179–1213.
[6] J. Sun, et al., Recent advances in cellulose nanofiber modification and characterization and cellulose Nanofiber-Based films for Eco-Friendly active food packaging, Foods 13 (24) (2024) 3999.
[7] C. Zinge, B. Kandasubramanian, Nanocellulose based biodegradable polymers, Eur. Polym. J. 133 (2020) 109758.
[8] M. Beg, et al., Biodegradable biopolymers for electrochemical energy storage devices in a circular economy, RSC Sustain. (2025).
[9] L. Ranakoti, et al., Critical review on polylactic acid: properties, structure, processing, biocomposites, and nanocomposites, Materials 15 (12) (2022) 4312.
[10] W. Limsukon, R. Auras, S. Selke, Hydrolytic degradation and lifetime prediction of poly (lactic acid) modified with a multifunctional epoxy-based chain extender, Polym. Test. 80 (2019) 106108.
[11] S. Farah, D.G. Anderson, R. Langer, Physical and mechanical properties of PLA, and their functions in widespread applications—a comprehensive review, Adv. Drug Deliv. Rev. 107 (2016) 367–392.
[12] J.S. Lyu, J.-S. Lee, J. Han, Development of a biodegradable polycaprolactone film incorporated with an antimicrobial agent via an extrusion process, Sci. Rep. 9 (1) (2019) 20236.
[13] M. Suzuki, Y. Tachibana, K.-i Kasuya, Biodegradability of poly (3-hydroxyalkanoate) and poly (ε-caprolactone) via biological carbon cycles in marine environments, Polym. J. 53 (1) (2021) 47–66.
[14] Y. Huang, et al., Effect of NR on the hydrolytic degradation of PLA, Polym. Degrad. Stab. 98 (5) (2013) 943–950.
[15] B. Lu, et al., Comparison of PCL degradation in different aquatic environments: effects of bacteria and inorganic salts, Polym. Degrad. Stab. 150 (2018) 133–139.
[16] J. Zheng, S. Suh, Strategies to reduce the global carbon footprint of plastics, Nat. Clim. Change 9 (5) (2019) 374–378.
[17] X. Sun, et al., Life cycle assessment of cellulose nanocrystals prepared from crop straw by sequential periodate-chlorite oxidation, Ind. Crops Prod. 214 (2024) 118596.
[18] P.G. Ponnusamy, S. Mani, Life cycle assessment of manufacturing cellulose nanofibril-reinforced chitosan composite films for packaging applications, Int. J. Life Cycle Assess. 27 (3) (2022) 380–394.
[19] C. Ingrao, et al., Polylactic acid trays for fresh-food packaging: a carbon footprint assessment, Sci. Total Environ. 537 (2015) 385–398.
[20] S. Sepahvand, et al., Recent developments in nanocellulose-based aerogels as air filters: a review, Int. J. Biol. Macromol. 246 (2023) 125721.
[21] S. Zong, et al., Construction of nanocellulose aerogels with environmental drying strategy without organic solvent displacement for High-Efficiency solar steam generation, ACS Nano 19 (5) (2025) 5305–5315.
[22] S. Ahankari, et al., Recent developments in nanocellulose-based aerogels in thermal applications: a review, ACS Nano 15 (3) (2021) 3849–3874.
[23] I. Turhan Kara, et al., Life cycle assessment of aerogels: a critical review, J. Sol. Gel Sci. Technol. 111 (2) (2024) 618–649.
[24] A. Ashori, S. Sepahvand, M. Jonoobi, Development of biodegradable nanofiber filters based on surface-modified cellulose nanofibers with graphene oxide for high removal of airborne particulate matter, Int. J. Biol. Macromol. 261 (2024) 129687.
[25] C. Zhang, et al., Graphene oxide-modified polyacrylonitrile nanofibrous membranes for efficient air filtration, ACS Appl. Nano Mater. 2 (6) (2019) 3916–3924.
[26] H. Chen, et al., Polyvinylidene fluoride/graphene oxide/polyimide composite high-efficiency PM 2.5 filtration nanofiber membranes, RSC Adv. 14 (24) (2024) 16828–16834.
[27] L. Liu, et al., Effect of sm doping on structure, dielectric properties and microwave absorption performance of SrMnO3, Ceram. Int. 50 (7) (2024) 12040–12049.
[28] S. Sadat Fazel, et al., Enhancing the oil adsorption properties of cellulose nanofiber aerogels through chemical modification, J. Polym. Environ. 32 (3) (2024) 1304–1313.
[29] S. Sepahvand, A. Ashori, M. Jonoobi, Cellulose nanofiber aerogels modified with titanium dioxide nanoparticles as high-performance nanofiltration materials, Int. J. Biol. Macromol. 256 (2024) 128204.
[30] A. Dutta, et al., Nanoporous air filtering systems made from renewable sources: benefits and challenges, Nanoscale 16 (32) (2024) 15059–15077.
[31] M. Zand, et al., Preparation and characterization of poly (vinyl pyrrolidone)/cellulose nanofiber/aloe vera composites as a biocompatible hydrating facial mask, Int. J. Biol. Macromol. 277 (2024) 133846.
[32] M. Khalid, et al., Green and sustainable electrospun poly (vinyl alcohol)/Eggshell nanofiber membrane with Lemon-Honey for facial mask development, ACS Omega 10 (13) (2025) 12972–12982.
[33] S. Sepahvand, et al., Surface modification of cellulose nanofiber aerogels using phthalimide, Polym. Compos. 41 (1) (2020) 219–226.
[34] H. Sai, et al., Surface modification of bacterial cellulose aerogels' web-like skeleton for oil/water separation, ACS Appl. Mater. Interfaces 7 (13) (2015) 7373–7381.
[35] Z. Wu, et al., Hydrophobic cellulose nanofiber based aerogel for high-efficiency oil-water separation, Int. J. Biol. Macromol. 305 (2025) 141173.
[36] A.T.K. Basti, et al., Employing cellulose nanofiber-based hydrogels for burn dressing, Polymers 14 (6) (2022) 1207.
[37] Y. Bas, et al., Preparation and characterization of softwood and hardwood nanofibril hydrogels: toward wound dressing applications, Biomacromolecules 24 (12) (2023) 5605–5619.
[38] G. Yang, et al., A cellulose nanofibril-reinforced hydrogel with robust mechanical, self-healing, pH-responsive and antibacterial characteristics for wound dressing applications, J. Nanobiotechnol. 20 (1) (2022) 312.
[39] M. Fukuhara, et al., Amorphous cellulose nanofiber supercapacitors, Sci. Rep. 11 (1) (2021) 6436.
[40] F. Erdem, H. Kandemir, F.B. Alp, Effect of polycaprolactone, zinc oxide, and poly (ethylene glycol) on the properties of polylactic acid composite fibers obtained by melt electrospinning, ACS Omega (2025).
[41] J. Zhao, et al., Preparation method and application of porous poly (lactic acid) membranes: a review, Polymers 16 (13) (2024) 1846.
[42] N.D. Bikiaris, et al., Recent advances in the investigation of poly (lactic acid)(PLA) nanocomposites: incorporation of various nanofillers and their properties and applications, Polymers 15 (5) (2023) 1196.
[43] M. Beg, et al., Paper supercapacitor developed using a manganese Dioxide/Carbon black composite and a water hyacinth cellulose Nanofiber-Based bilayer separator, ACS Appl. Mater. Interfaces 15 (44) (2023) 51100–51109.
[44] N. Herrera, P. Olsen, L.A. Berglund, Strongly improved mechanical properties of thermoplastic biocomposites by PCL grafting inside holocellulose wood fibers, ACS Sustain. Chem. Eng. 8 (32) (2020) 11977–11985.
[45] J. Pang, et al., Wood cellulose nanofibers grafted with poly (ε-caprolactone) catalyzed by ZnEu-MOF for functionalization and surface modification of PCL films, Nanomaterials 13 (13) (2023) 1904.
[46] R.A. Ilyas, et al., Natural-fiber-reinforced chitosan, chitosan blends and their nanocomposites for various advanced applications, Polymers 14 (5) (2022) 874.
[47] J.Y. Boey, C.K. Lee, G.S. Tay, Factors affecting mechanical properties of reinforced bioplastics: a review, Polymers 14 (18) (2022) 3737.
[48] T. Zhou, et al., Mechanical performance and thermal stability of polyvinyl alcohol–cellulose aerogels by freeze drying, Cellulose 26 (3) (2019) 1747–1755.
[49] A. Benkaddour, et al., Grafting of polycaprolactone on oxidized nanocelluloses by click chemistry, Nanomaterials 3 (1) (2013) 141–157.
[50] J.P. Mofokeng, et al., Comparison of injection moulded, natural fibre-reinforced composites with PP and PLA as matrices, J. Thermoplast. Compos. Mater. 25 (8) (2012) 927–948.
[51] S. Eshraghi, S. Das, Mechanical and microstructural properties of polycaprolactone scaffolds with one-dimensional, two-dimensional, and three-dimensional orthogonally oriented porous architectures produced by selective laser sintering, Acta Biomater. 6 (7) (2010) 2467–2476.
[52] M. Bijarimi, et al., Biodegradable binary blend of poly (lactic acid)/polypropylene via twin-screw extruder: preparation and characterization. AIP Conference Proceedings, AIP Publishing, 2021.
[53] C. Baptista, et al., The effect of temperature and pressure on polycaprolactone morphology, Polymer 191 (2020) 122227.
[54] R. Zhang, et al., Glass transition temperature of poly (d, l-lactic acid) of different molar mass, Thermochim. Acta 718 (2022) 179387.